

Fixed-node errors in quantum Monte Carlo: interplay of electron density and node nonlinearities

Kevin M. Rasch, Shuming Hu, Lubos Mitas
Center for High Performance Simulation and Department of Physics,
North Carolina State University, Raleigh, NC 27695
 (Dated: February 26, 2022)

We elucidate the origin of large differences (two-fold or more) in the fixed-node errors between the first- vs second-row systems for single-configuration trial wave functions in quantum Monte Carlo calculations. This significant difference in the fixed-node biases is studied across a set of atoms, molecules, and also Si, C solid crystals. The analysis is done over valence isoelectronic systems that share similar correlation energies, bond patterns, geometries, ground states, and symmetries. We show that the key features which affect the fixed-node errors are the differences in electron density and the degree of node nonlinearity. The findings reveal how the accuracy of the quantum Monte Carlo varies across a variety of systems, provide new perspectives on the origins of the fixed-node biases in electronic structure calculations of molecular and condensed systems, and carry implications for pseudopotential constructions for heavy elements.

PACS numbers: 02.70.Ss, 71.15.-m, 31.15.V-

Quantum Monte Carlo (QMC) approaches have proven to be remarkably successful in studies of many-body quantum systems. For electronic structure calculations, QMC offers an important alternative [1, 2] to approaches based on either density functional theory (DFT) or basis set correlated wave function methods. The fundamental inefficiency of fermion signs in QMC can be overcome by the fixed-node approximation in which the node (zero locus) of a desired stationary eigenstate is constrained to be identical to the node of the best available trial wave function. It is very encouraging that commonly used Slater-Jastrow trial wave functions enable us to recover about 90-95% of the correlation energy almost universally, in atoms, molecules, solids, quantum liquids, etc. Energy differences produced by this “QMC standard model,” such as bindings/cohesions, reaction barriers, and excitations, for example, agree with experiments within a few percent for many systems and elements across the periodic table [1, 2].

Despite these achievements, the fixed-node error remains the key limiting factor in the quest for higher systematic accuracy and in studies of quantum phenomena at finer energy scales. Several methods for improving nodal hypersurfaces have been proposed (see, e.g., ideas in recent Ref. [3]), however, it is fair to say that such effort is almost invariably very demanding and often not fundamentally different from slowly converging wave function expansions in excitations. Our understanding of the nodal hypersurfaces is still very rudimentary and other than insights into topologies of nodal cells [4–6], many aspects of these remain unknown. Therefore, identifying the source of the nodal inaccuracies in the most commonly used variational wave functions is perhaps the most important outstanding question.

Recently, high-accuracy QMC calculations showed a striking difference between the fixed-node errors of Si₂

vs C₂ dimers [7]. Interestingly, this turned out to be just a special case of a broader and more systematic trend. As we show below, for commonly used single-configuration Slater-Jastrow trial functions, the fixed-node errors of the first- vs second-row atom systems systematically differ by a significant amount, i.e., by a factor of two or more. This difference persists in atoms, molecules, and solids despite the fact that the compared systems have identical ground states and symmetries, similar bonding patterns, geometric structures, valence correlation energies, and even qualitatively similar excitation spectra. Our analysis of this effect is built on recent findings that in simple atomic systems the nodal errors grow in proportion to the electronic density [8] (and similar result was found for homogeneous electron gas [9] with the error being proportional to $\ln r_s$). Ultimately, we reveal that besides the electron density, the fixed-node biases are strongly affected by the node nonlinearities. These nonlinearities originate from the different degree of localization of occupied states in different symmetry channels, and they are further affected by bonding patterns and bond multiplicities. Our findings have rather wide implications for systems composed from main group elements, 3d transition metals, and beyond. Our analysis has potential implications also for construction of pseudopotentials which can alleviate some of these effects in heavier elements.

QMC calculations. Total energies of a selected set of first- and second-row systems have been calculated by fixed-node diffusion Monte Carlo (FNDMC) with single-configuration Slater-Jastrow trial functions. The only exception was the C atom, where we included two configurations due to the known and sizable $s^2 \rightarrow p^2$ near-degeneracy, which does not affect the rest of compared systems (e.g., in the Si atom it is below ≈ 1 mHa).

For generating one-particle orbitals we have employed

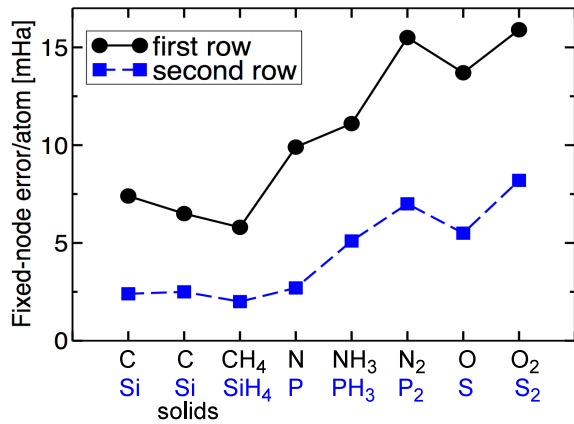


FIG. 1: Fixed-node errors of the single-configuration trial wave functions for a set of first- and second-row atoms, dimers, hydrides and the diamond structure solids of C and Si. The values are normalized per non-hydrogen atom.

Hartree-Fock (HF) and several DFT functionals, including hybrids; and for each system we have chosen the orbital set with the lowest fixed-node energy. For all elements except hydrogen, we have used the energy consistent pseudopotentials (PPs) [10] and basis sets of the cc-pV5Z quality. Our total energies are similar to or marginally higher than (1mHa or less) the recent high-accuracy calculations of the G2 benchmark set of molecules that additionally included explicit QMC orbital reoptimizations [11]. QMC calculations of the C and Si solids in the diamond structure were done with 8- and 64-atom supercells with twisted averaging, extrapolation to the thermodynamic limit using the $S(\mathbf{k})$ correction [12], and for the Si crystal we verified that 216-atom supercell result was consistent with the extrapolation.

Estimation of the exact total energies. For an independent estimation of the exact total valence energies with the target accuracy of 1mHa/atom (or better) in atoms and molecules, we have carried out CCSD(T) calculations with ccpVnZ basis sets with $2 \leq n \leq 5$ and extrapolated to $n \rightarrow \infty$. The extrapolation formula was based on the sum of two contributions: exponential for the HF energy component and sum of power terms $c_1 n^{-3} + c_2 n^{-5}$ for the correlation [13]. This formula provided very good agreement with ours and also previously reported high-accuracy, multi-reference FNDMC calculations for selected systems such as N, C atoms and N₂ dimer [7, 14]. We found the results to agree within ≈ 0.6 mHa. Solely for the C and Si solids, we estimated the exact total energies with empirical inputs, using the experimental cohesive energies corrected for the zero-point motion.

Fixed-node errors. The resulting fixed-node errors are summarized in Fig. 1. The chosen first- and second-row systems are directly comparable, i.e., they are valence iso-

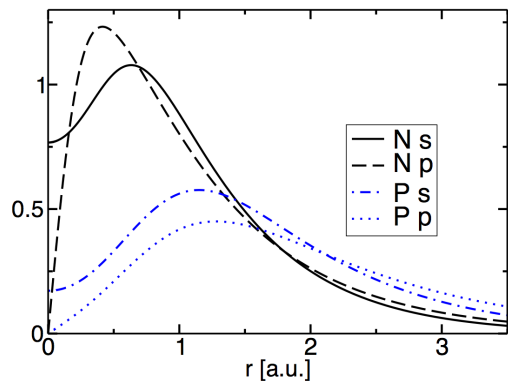


FIG. 2: Radial parts of $s(\ell = 0)$ and $p(\ell = 1)$ valence PP orbitals plotted as $r^\ell \rho_\ell(r)$ for the N and P atoms.

electronic, share very similar geometries, bond patterns and have the same ground states and symmetries. Except for the atoms, we mostly present closed-shell states in order to simplify the analysis although the effect persists in open-shell states as well (e.g., C₂ vs Si₂ shows such a difference as well and is only further enhanced by the multi-reference C₂ ground state [7]). Our first key observation is that all the fixed-node errors for the first row are systematically and significantly higher than for the second row. Remarkably, this is true not only for atoms and molecules but also for the Si and C crystals.

The results in Fig. 1 raise a natural question: what is the reason for this trend? First, we consider the fact that the valence correlation energies are larger in the first row. They differ only moderately, by about 20% or less. For example, the correlation energy of the N atom is ≈ 134 mHa while for the P atom it is ≈ 120 mHa, i.e., about 10% difference. However, this does not explain why the fixed-node error for P is only ≈ 2.5 mHa ($\approx 2\%$ E_{corr}), while for N it is ≈ 10 mHa ($\approx 8\%$ of E_{corr}), i.e., the difference is four times larger both in absolute and relative terms. The multi-reference character of the states is not an issue either since most of the studied cases exhibit large gaps and the wave functions are nominally of the single-reference type. Also note that excitations in P₂ lie lower than in N₂, but the error is much larger in the latter case. That is counterintuitive since one would expect more pronounced effects and mixing due to the smaller gap of P₂. Another suggestion would be to look at pseudopotentials as the source of the differences. As we will see below, pseudopotentials can and do influence the results, but they are *not* the root cause.

Let us then focus on the key qualitative difference between the two rows, i.e., the absence of p -states in cores of the first row. For these elements the p -states are much more localized in the region close to nucleus, in particular, the orbital maximum appears at a smaller radius and is higher than for the s -states. The opposite is true for main elements in the second row (and rows below),

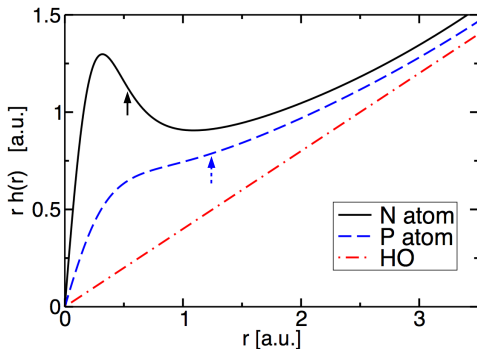


FIG. 3: The functions $rh(r) = r\rho_p(r)/\rho_s(r)$ for N atom, P atom and harmonic oscillator fermions. The small arrows indicate the core radii of N atom (0.55 au) and P atom (1.27 au) defined as the outermost maximum of the one-particle electron density.

see the examples of N and P atoms in Fig. 2.

The simplest nodes model and nodal analysis. We analyze the impact of the spatial character of s, p states on the nodes starting from the example of non-interacting 3D harmonic fermions. This choice is motivated by the fact that this is perhaps the simplest solvable model of nodes in localized systems (the nodes turn out to be zeros of homogeneous antisymmetric polynomials [6]). It also enables us to construct states with the same symmetries as few-electron atoms. Let us therefore write the harmonic oscillator (HO) one-particle orbitals as $g(r), g(r)x, g(r)y, \dots$ where $g(r)$ is a gaussian. The simplest state with the fermion node is the two-electron triplet ${}^3P(sp)$ and has the wave function

$$\Psi_{HO}(1, 2) = g(r_1)g(r_2)\det[1, x] = G_0(x_2 - x_1),$$

where the gaussians are absorbed into the non-negative prefactor G_0 . The node is $x_1 = x_2$, and the gradient of the antisymmetric factor is constant so that the node is flat. For more electrons, the wave function has the same form: non-negative prefactor times a homogeneous antisymmetric polynomial with the node being its zero locus.

Let us now reanalyze the same ${}^3P(sp)$ state using one-particle orbitals given as $\rho_s(r), \rho_p(r)x, \dots$ from wave functions of the pseudized first- and second-row atoms. By dividing out the nonnegative $\rho_s(r)$, we get

$$\Psi_{atom}(1, 2) = \tilde{G}_0 \times [h(r_2)x_2 - h(r_1)x_1],$$

i.e., the non-negative prefactor times the antisymmetric part, where $h(r) = \rho_p(r)/\rho_s(r)$. For simplicity, let us now assume that the particles 1 and 2 are confined to the x -axis. It is then quite revealing to plot the function $h(|x|x) \equiv h(r)r$. Fig. 3 shows this function for the N, P atoms and HO (rescaled by multiplicative constants for a better comparison). Clearly, for HO it is linear since the

corresponding $h(r) = 1$. For the P atom the function deviates from linearity, however, the key observation is that it remains *monotonous*. This implies that there is only one set of configurations which fulfills the nodal condition $r_1h(r_1) = r_2h(r_2)$, qualitatively the same as for HO. The nodes of these two systems are therefore similar, with some deviation from flatness in the P case. However, this contrasts with $rh(r)$ for N which shows a distinctly different behavior, with a pronounced maximum at $r \approx 0.35$ au and a minimum around $r \approx 1.15$ au. It is important to note that the nonlinearity spans well beyond the core radius defined as the outermost maximum of the one-particle electronic density. Therefore this feature has its root in the all-electron structure since beyond the core radius the (pseudo) orbitals and also $h(r)$ functions are virtually identical to their all-electron counterparts. The pseudopotential merely smoothes out their behavior inside the core. Clearly, similar nonlinearities generated by $2s$ and $2p$ states are present in the second-row atoms. The key difference is that these effects are fully contained in the core while for the first row they *unavoidably extend well into the bonding region*.

This nonlinearity has a significant impact on the nodal structure of the wave function. In particular, for certain ranges of positions of electrons 1 and 2, there are multiple sets of configurations for which the wave function vanishes. When compared to HO, the nonlinearity of $rh(r)$ suggests that the wave function qualitatively corresponds to an antisymmetric polynomial of higher degree and the complexity of its nodal shape grows accordingly. This analysis can be extended to include the rest of the electrons in full 3D space and one finds that the first-row systems exhibit complicated nodal shapes. For certain configurations, distortions appear in the form of bulges and even detached bubbles, see Fig. 4. In this Figure, we show a 3D subset of the node found by 3D scan of the trial function by one majority-spin electron with the rest of the electrons fixed at snapshot positions. These nonlinear features have high curvatures and are also sensitive to interactions since they are not “held in place” by the other electrons.

One might argue that such nonlinearities affect only small regions of configurations and since the wave function vanishes at the node the impact on expectations should be small as well. However, this argument is not strictly correct, especially if we are interested in the last few percent of the correlation energy. One can show that the wave function nonlinearities at the node are ultimately related to the wave function values elsewhere and therefore have an impact on the total energy. Recently, we have proposed to write [15] the total energy of an exact many-body eigenstate Ψ_0 for a general potential $V(\mathbf{R})$ as follows

$$E_0 = \left[\int_{\partial\Omega} |\nabla\Psi_0| d\mathbf{S} + \int V(\mathbf{R}) |\Psi_0| d\mathbf{R} \right] / \int |\Psi_0| d\mathbf{R}$$

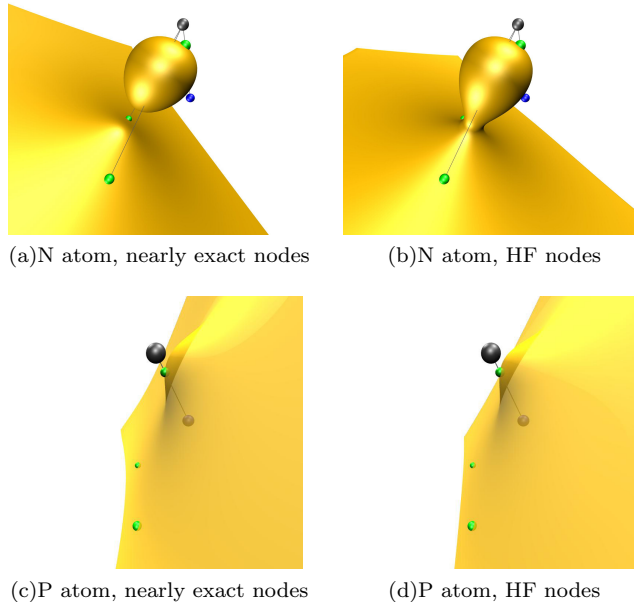


FIG. 4: High curvature nodal features of the N and P atoms from 3D scans by a majority spin electron for HF and multi-reference (nearly exact, ≈ 1 mHa) wave functions. The larger (black) spheres are the nuclei while the smaller spheres are snapshot positions of the rest of electrons (green/blue for the majority/minority spin). The fixed electrons are at the corresponding positions (radially adjusted according to the core radii) for both atoms but their nodes are dramatically different. In addition, the N atom node is much more sensitive to interactions as seen from the difference between the two wave functions.

where the first integral is over the nodal (hyper)surface $\partial\Omega$ while the other integrals are over the particle coordinates. Note that these are not usual expectations since the averages are over $|\Psi_0|$, $|\nabla\Psi_0|$. Instead, the “kinetic” component is more sensitive to the nodal features since it depends on the node (hyper)area and on the gradient of the wave function at the node locus. As we have shown elsewhere [15], this diagnostics has enabled us to distinguish between two different nodal surfaces for degenerate states as well as to show, for example, equivalency of nodal surfaces for two states with different symmetries. Estimation of these components in QMC reveals that the first term for the N atom is approximately 3.3 times larger than for the P atom, reflecting thus the node differences in a quantitative manner. Note that atomic errors rise very significantly with the double occupation of p -states (for example, O and S atoms), confirming that the impact of the electron density increase is qualitatively similar in both rows.

Systems with bonds. Since bonding affects both the density and molecular orbitals, one expects that the nodal errors will be influenced by the degree of node nonlinearity and by the density changes from the bond ge-

ometries. In particular, for Si systems with tetrahedral bonding, the errors are only about 2% of the correlation energy. This is true for *both* the silane and the solid. In addition, we claim that this will hold also in other Si systems with tetrahedral arrangements of single bonds such as Si_2H_6 , etc. Single bonds arrangements and low overall density therefore appears to decrease the corresponding fixed-node errors. Moreover, we expect this to be true basically for all such IV-group element systems below the first row! On the other hand, the errors grow with shortening of the single bonds in NH_3 , PH_3 , and they are the largest in systems with multiple bonds and high densities such as N_2 . It is instructive to roughly estimate how much of the molecular errors originate in atoms and how much result from multiple bonds and associated effects. Assuming that the errors are approximately additive, the effect of multiple bonds in N_2 is $\epsilon_{mol} - 2\epsilon_{at} \approx 32 - 2 \times 10 = 12 \text{ mHa}$, while for P_2 we get $\approx 14 - 2 \times 2.5 = 9 \text{ mHa}$. The smaller value for P_2 reflects the longer bond length, smaller density, and correspondingly smaller orbital curvatures. It is not too difficult to accept that *qualitatively* the multiple bonds not only raise the density but also increase the degree of the node nonlinearity. In particular, the “stacking” of multiple bonding - and also antibonding orbitals which have significant densities along the bond axis - can be approximately described as a polynomial with a higher degree than in isolated atoms. In contrast, note that the tetrahedral single bond arrangement does not increase the nodal error, for example, in methane and diamond. As argued above, this arrangement appears to be “optimal” and the existing nodal bias comes almost exclusively from the atoms, for both Si and C such systems.

Conclusions. We have shown that fixed-node errors in atoms and bonded systems are influenced mainly by two factors: the high electronic density and the node nonlinearity in such regions. In particular, we have found that: a) the first-row atoms exhibit node nonlinearities that significantly raise the fixed-node errors, due to the high density of p -states close to nuclei; b) for the main group elements in the second-row and below this effect is almost absent; c) in bonded systems the fixed-node bias grows with shorter bonds and higher bond multiplicities. Perhaps the most far-reaching conclusion is that the contrast between the fixed-node bias of the first vs the second rows and rows beyond, holds for *all* main group (sp) elements across the periodic table. In particular, for atoms and tetrahedral bonded systems of Si (Ge, ...) the fixed-node errors amount to only $\approx 2\%$ of E_{corr} . The results also suggest that the $3d$ transition elements exhibit similar effects although they are mostly confined to the core region so that systems with $p-d$ bonds exhibit quite accurate energy differences due to error cancellations [16]. In addition, we envision that for heavier elements the atomic node nonlinearities can be alleviated by properly adjusted pseudopotential constructions.

We believe that our analysis provides a new perspective on the origins of the fixed-node biases, reveals why the accuracy of fixed-node QMC calculations varies for different types of systems, and offers hints on future opportunities to address this fundamental challenge.

Acknowledgments. We would like to thank M. Bajdich for his efforts in the very early stages of this work. We acknowledge support by NSF OCI-0904794 and ARO W911NF-04-D-0003-0012 grants and by XSEDE computer time allocation at TACC.

-
- [1] W. M. C. Foulkes, L. Mitas, R. J. Needs, and G. Rajagopal, *Rev. Mod. Phys.* **73**, 33 (2001).
 - [2] J. Kolorenc and L. Mitas, *Rep. Prog. Phys.* **74**, 026502 (2011).
 - [3] F. A. Reboredo, R. Q. Hood, and P. R. C. Kent, *Phys. Rev. B*, **79**, 195117 (2009).
 - [4] D.M. Ceperley, *J. Stat. Phys.*, **63**, 1237 (1991).
 - [5] D. Bressanini and P.J. Reynolds, *Phys. Rev. Lett.* **95**, 110201 (2005).
 - [6] L. Mitas, *Phys. Rev. Lett.* **96**, 240402 (2006).
 - [7] C. J. Umrigar, J. Toulouse, C. Filippi, S. Sorella, and R. G. Hennig, *Phys. Rev. Lett.* **98**, 110201 (2007).
 - [8] K.M. Rasch and L. Mitas, *Chem. Phys. Lett.*, **528**, 59 (2012); A. Kulahlioglu and L. Mitas, submitted.
 - [9] J.J. Shepherd, A. Gruneis, G.H. Booth, G. Kresse, and A. Alavi, *Phys. Rev. B* **86**, 035111 (2012); J.J. Shepherd, G. Booth, A. Gruneis, and A. Alavi, *Phys. Rev. B* **85**, 081103 (2012); J.J. Shepherd, A. Alavi, private communication.
 - [10] M. Burkatzki, C. Filippi, and M. Dolg, *J. Chem. Phys.* **126**, 234105 (2007).
 - [11] F. R. Petruzielo, J. Toulouse, C. J. Umrigar, *J. Chem. Phys.* **136**, 124116 (2012).
 - [12] S. Chiesa, D. M. Ceperley, R. M. Martin, and M. Holzmann, *Phys. Rev. Lett.* **97**, 076404 (2006).
 - [13] D. Feller, K. A. Peterson, and J. G. Hill, *J. Chem. Phys.* **135**, 044102 (2011).
 - [14] M. Bajdich, M. L. Tiago, R. Q. Hood, P. R. C. Kent, and F. A. Reboredo, *Phys. Rev. Lett.* **104**, 193001 (2010).
 - [15] S. Hu, K. M. Rasch, and L. Mitas, in *Advances in Quantum Monte Carlo*, edited by S. Tanaka, S. M. Rothstein, W. A. Lester, Jr., ACS Symposium Series, Vol. 1094, 2012, pp. 77.; arXiv:1307.5567.
 - [16] J. Kolorenc and L. Mitas, *Phys. Rev. Lett.* **101**, 185502 (2008).